LAWRENCE
LIVERMORE
NATIONAL
LABORATORY

LLNL-PROC-457057

Synergy Between Lithium Plasma-Facing Component Coatings and the Snowflake Divertor Configuration in NSTX

V. A. Soukhanovskii, J. Ahn, M. G. Bell, R. E. Bell, D. A. Gates, S. Gerhardt, R. Kaita, E. Kolemen, H. W. Kugel, B. P. LeBlanc, R. Maqueda, A. McLean, J. E. Menard, D. Mueller, S. F. Paul, A. Y. Pigarov, R. Raman, T. Rognlien, A. L. Roquemore, D. D. Ryutov, S. A. Sabbagh, R. Smirnov, D. P. Stotler

September 27, 2010

23rd IAEA Fusion Energy Conference
Daejon, South Korea
October 11, 2010 through October 16, 2010

Disclaimer

OVERVIEW OF PHYSICS RESULTS FROM NSTX

R. Raman 1), J-W. Ahn 2), J. Allain 3), R. Andre 4), R. Bastasz 5), D. Battaglia 2), P. Beiersdorfer 6), M. Bell 4), R. Bell 4), E. Belova 4), J. Berkery 7), R. Betti 4,8), J. Bialek 7), T. Bigelow 2), M. Bitter 4), J. Boedo 9), P. Bonoli 10), A. Boozer 7), A. Bortolon 11), D. Brennan 12), J. Breslau 4), R. Buttery 13), J. Canik 2), G. Caravelli 14), C. Chang 15), N.A. Crocker 16), D. Darrow 4), B. Davis 4), L. Delgado-Aparicio 4), A. Diallo 4), S. Ding 17), D. D'Ippolito 18), C. Domier 11), W. Dorland 19), S. Ethier 4), T. Evans 13), J. Ferron 13), M. Finkenthal 14), J. Foley 20), R. Fonck 21), R. Frazin 22), E. Fredrickson 4), G. Fu 4), D. Gates 4), S. Gerhardt 4), A. Glasser 1), N. Gorelenkov 4), T. Gray 2), Y. Guo 17), W. Guttenfelder 4), T. Hahm 4), R. Harvey 23), A. Hassanein 3), W. Heidbrink 24), K. Hill 4), Y. Hirooka 25), E.B. Hooper 6), J. Hosea 4), B. Hu 8), D. Humphreys 13), K. Indireshkumar 4), F. Jaeger 2), T. Jarboe 1), S. Jardin 4), M. Jaworski 4), R. Kaita 4), J. Kallman 4), O. Katsuro-Hopkins 7), S. Kaye 4), C. Kessel 4), J. Kim 26), E. Kolemen 4), S. Krasheninnikov 9), S. Kubota 16), H. Kugel 4), R. LaHaye 13), L. Lao 13), B. LeBlanc 4), W. Lee 26), K. Lee 11), J. Leuer 13), F. Levinton 20), Y. Liang 11), D. Liu 24), N. Luhmann Jr. 11), R. Maingi 2), R. Majeski 4), J. Manickam 4), D. Mansfield 4), R. Maqueda 20), E. Mazzucato 4), A. McLean 2), D. McCune 4), B. McGeehan 27), G. McKee 21), S. Medley 4), J. Menard 4), M. Menon 28), H. Meyer 29), D. Mikkelsen 4), G. Miloshevsky 3), D. Mueller 4), T. Munsat 30), J. Myra 18), B. Nelson 1), N. Nishino 31), R. Nygren 5), M. Ono 4), T. Osborne 13), H. Park 26), J. Park 4), S. Paul 4), W. Peebles 16), B. Penaflor 13), C. Phillips 4), A. Pigarov 9), M. Podesta 4), J. Preinhaelter 32), Y. Ren 4), H. Reimerdes 7), G. Rewoldt 4), P. Ross 4), C. Rowley 4), E. Ruskov 24), D. Russell 18), D. Ruzic 22), P. Ryan 2), S.A. Sabbagh 7), M. Schaffer 13), E. Schuster 33), F. Scotti 4), K. Shaing 21), V. Shevchenko 29), K. Shinohara 34), V. Sizyuk 3), C.H. Skinner 4), A. Smirnov 23), D. Smith 21), P. Snyder 13), W. Solomon 4), A. Sontag 2), V. Soukhanovskii 6), T. Stoltzfus-Dueck 4), D. Stotler 4), B. Stratton 4), D. Stutman 14), H. Takahashi 4), Y. Takase 35), N. Tamura 25), X. Tang 36), G. Taylor 4), C. Taylor 3), K. Tritz 14), D. Tsarouhas 3), M. Umansky 6), J. Urban 32), E. Utergberg 13), M. Walker 13), W. Wampler 5), W. Wang 4), J. Whaley 5), R. White 4), J. Wilgen 2), R. Wilson 4), K.L. Wong 4), J. Wright 10), Z. Xia 11), D. Youchison 5), G. Yu 9), H. Yuh 20), L. Zakharov 4), D. Zemlyanov 3), G. Zimmer 4), S.J. Zweben 4)

1) University of Washington, Seattle, WA, USA
2) Oak Ridge National Laboratory, Oak Ridge, TN, USA
3) Purdue University, Purdue, IA, USA
4) Princeton Plasma Physics Laboratory, Princeton, NJ, USA
5) Sandia National Laboratory, Albuquerque, NM, USA
6) Lawrence Livermore National Laboratory, Livermore, CA, USA
7) Columbia University, New York, NY, USA
8) University of Rochester, Rochester, NY, USA
9) University of California at San Diego, San Diego, CA, USA
10) Massachusetts Institute of Technology, Cambridge, MA, USA
11) University of California at Davis, Davis, CA, USA
12) University of Tulsa, Tulsa, OK, USA
13) General Atomics, San Diego, CA, USA
14) Johns Hopkins University, Baltimore, MD, USA
15) New York University, New York, NY, USA
16) University of California at Los Angeles, Los Angeles, CA, USA
17) Academia Sinica Institute of Plasma Physics, Hefei, Anhui, China
18) Lodestar Research Corporation, Boulder, CO, USA

19) University of Maryland, College Park, MD, USA
20) Nova Photonics, Inc., Princeton, NJ, USA
21) University of Wisconsin-Madison, Madison, WI, USA
22) University of Illinois at Urbana-Champaign, Urbana, IL, USA
23) CompX , Del Mar, CA, USA
24) University of California at Irvine, Irvine, CA, USA
25) NIFS, Oroshi, Toki, Gifu, Japan
26) POSTECH, Pohang, Korea
27) Dickinson College, Carlisle, PA, USA
28) Think Tank Inc., Silver Springs, MD, USA
29) UKAEA Culham Science Center, Abingdon, Oxfordshire, UK
30) University of Colorado at Boulder, Boulder, CO, USA
31) Hiroshima University, Hiroshima, Japan
32) Institute of Plasma Physics, AS CR, Prague, Czech Republic
33) Lehigh University, Bethlehem, PA, USA
34) JAEA, Naka, Ibaraki, Japan
35) University of Tokyo, Tokyo, Japan
36) Los Alamos National Laboratory, Los Alamos, NM, USA

Abstract. During the last two experimental campaigns, the low aspect-ratio NSTX has explored physics issues critical to both toroidal confinement physics and ITER. Experiments have made extensive use of both lithium coatings for wall conditioning, n = 1 resistive wall mode control, and non-axisymmetric field correction to reliably produce high-performance neutral-beam heated discharges with non-inductive current fractions up to 0.70, extending to 1.7 s in duration. The resistive wall mode control coils have been used to trigger repetitive ELMs with high reliability and have also contributed to an improved understanding of both neoclassical tearing mode and resistive wall mode stabilization physics, including the interplay between rotation and kinetic effects in stability. High Harmonic Fast Wave (HHFW) heating produced plasmas with central electron temperatures exceeding 6 keV. The HHFW was used to show that there was little difference in power threshold for the L–H transition for D and He plasmas, which suggests that operation in helium may be the best approach to developing H-mode scenarios in the early non-nuclear phase of ITER operation. A new fast ion diagnostic showed a depletion of the fast ion profile over a broad spatial region as a result of toroidicity-induced Alfvén eigenmodes (TAE) and energetic particle modes (EPM) bursts. In addition, it was observed that other modes (e.g. Global Alfvén eigenmodes) can trigger TAE and EPM bursts, suggesting redistribution of fast ions by high-frequency AEs. The momentum pinch velocity determined by a perturbative technique decreased as the collisionality was reduced. The processes governing deuterium retention by graphite and lithium-coated graphite plasma facing components (PFCs) have been investigated. To reduce divertor heat flux, a novel divertor configuration, called the "snowflake" divertor was tested in NSTX and many beneficial aspects were found. A reduction in the required central solenoid flux has been realized in NSTX when discharges initiated by coaxial helicity injection were ramped in current using induction and have produced the type of plasma needed to meet the objectives of the non-inductive start-up and ramp-up program of NSTX.

1. Introduction

The National Spherical Torus Experiment (NSTX) produces plasmas with toroidal aspect ratio, that is, the ratio of the plasma major radius to its minor radius, as low as 1.25. These plasmas can be heated by up to 6 MW radio-frequency (RF) waves and 7 MW of deuterium Neutral Beam Injection (NBI). The plasmas in NSTX are surrounded by closely fitting conducting plates to inhibit the development of instabilities driven by the plasma pressure. The poloidal field coils provide flexible plasma shaping and a set of six non-axisymmetric external coils provide for correction of field errors and feedback control of some plasma instabilities. Results from the six basic science topical groups in NSTX are covered in the following sections: 2) Macrostability physics, 3) Transport and Turbulence Physics, 4) Boundary Physics and Lithium Research, 5) Waves and Fast Particle Physics, 6) Solenoid Free Startup, and 7) Advanced Scenarios and Control. Work conducted in support of ITER research is covered within the above areas.

2. Macrostability Physics

2.1 RWM control physics and beta feedback control at varied rotation

NSTX routinely operates with normalized-beta, $\beta_N = \beta_T/(I_p/aB_T)$ (units of %.m.T/MA) substantially above the n = 1 no-wall ideal stability limit. These plasmas are susceptible to the growth of resistive wall modes (RWM) unless stabilizing plasma rotation profiles can be maintained. Operation at steady, high β_N is desired for fusion energy applications. To address this need, combined n = 1 RWM and newly-implemented β_N feedback was achieved at various plasma rotation levels [1]. High pulse-averaged β_N was maintained with low levels of β_N fluctuation. Fluctuations in NBI power are feedback controlled to maintain constant β_N, but not plasma rotation. Despite this, the toroidal rotation in the outer plasma reaches approximate steady state in these plasmas. Specifically, increasing NBI heating increases the drive torque for plasma rotation, as well as increasing plasma β_N and T_i. Increasing β_N increases both the plasma amplification of the applied field and T_i. Each of these leads to an increase in neoclassical toroidal viscosity braking torque [2]. As NBI varies, the changes in the driving and braking torques tend to offset each other, producing almost steady plasma rotation. The RWM control coils are now routinely used to compensate an intrinsic, slowly varying n = 3 field error [3]. The correction of this field error improves plasma performance by allowing steady and rapid toroidal rotation. Experiments confirmed that the previously observed n=3 error field is due to a non-circularity in the main vertical field coil [4], and an improved correction scheme was found. The RWM sensors are now compensated for AC control fields and OHxTF pickup particularly important for the RWM radial field sensors. Favorable feedback phase and gain settings were found in controlled experiments for both the poloidal and radial field RWM sensor arrays (48 coils total). The RWM B_R sensor feedback phase setting for negative feedback agrees with theory, and these sensors are now routinely used. Dedicated experiments have shown high success in stabilizing long-pulse plasmas with near record ratios of β_N/l_i between 12 – 13 with high success, compared to equivalent plasmas produced last year which suffered RWM-induced disruptions in half of the shots run.

An advanced RWM state space controller was recently implemented that uses a reduced order model of the 3D conducting structure of NSTX and a high beta n = 1 ideal plasma instability eigenfunction [5]. Such a controller has been proposed for RWM stabilization in ITER, and has the potential of allowing improved RWM control with coils placed further from the plasma and partially shielded by conducting structure. In initial experiments, large resonant field amplification causing plasma disruption was sufficiently reduced to allow stable plasma operation. Superior controller settings produced a stable, long pulse (limited by magnet heating constraints), low internal inductance (l_i) plasma, β_N exceeding 6.4, and β_N/l_i exceeding 13 – a record high value for a stable plasma at high plasma current (I_p = 1MA) [1].

2.2 RWM passive stabilization physics

NSTX experiments have discovered that the RWM can become unstable at intermediate levels of plasma rotation, [6] significantly greater than reported in DIII-D [7]. Analysis has shown kinetic effects, including resonances with trapped and passing ion bounce and precession drift frequencies, are important for determining the plasma rotation level and profile required to stabilize the mode. [1,8] Numerical calculations of the influence of fast-ions on RWM stability have been performed with the MISK code [9] which computes the perturbed mode energy including kinetic effects using the unperturbed ideal-kink eigenfunction. These calculations predict that the RWM will become progressively more stable as the fast-ion pressure is increased. To test these predictions, experiments were performed in NSTX varying the fast-ion content by varying the plasma current and field at fixed safety factor, q, to change the plasma temperature and density and, thereby, the fast-ion slowing-down time. As expected, the fast-ion content measured by the Fast-Ion D-alpha (FIDA) diagnostic was significantly reduced for the plasma with lower field and current. A higher plasma rotation frequency was required to achieve stability to the RWM for the plasma with lower fast ion content, consistent with theoretical predictions that fast-ions are stabilizing for the RWM. The stabilization from energetic particles is theoretically predicted to be nearly independent of the plasma rotation frequency because the bounce and precession drift frequencies for energetic particles are much larger than the

plasma rotation frequency. Even with energetic particle stabilization, the RWM can still be driven unstable in a band of rotation between the stabilizing precession drift and bounce resonance frequencies. Low frequency MHD spectroscopy [10] was used as a technique to directly measure RWM stability in these plasmas by examining the resonant field amplification of a low amplitude n = 1 field. Discharges at nearly constant β_N and above the n = 1 ideal no-wall limit have indeed shown greater than a factor of two variation in RFA amplitude as the plasma rotation is slowed with profiles near the expected marginal stability condition.

2.3 Error field threshold in high beta plasmas

The "locking" of MHD modes to static magnetic perturbations is believed to be caused by the sudden opening of magnetic islands at the rational surfaces, when the external non-axisymmetric field is beyond a threshold and plasma rotation can no longer shield it. This can be followed by enhanced transport across magnetic islands and rotational damping, so islands can grow further leading ultimately to plasma disruption. Since external magnetic perturbations almost always exist in tokamak devices, it is important to estimate the field threshold for locking and to correct the field below the threshold. Estimating the actual driving field at the rational surfaces has been significantly improved by employing the IPEC code [11], which calculates the ideal plasma response, shielding currents and the total resonant field (δB_{mn}) at the rational surfaces where q = m/n. At increased β_N, the applied field can be amplified and thereby become more destructive. To explore this, perturbing n = 1 fields were applied to the plasma with varying phases, application times, and ramp rates. These scans were repeated for three target discharges designed to provide a scan over β_N. At high values, using only the vacuum field, the error-field penetration occurred at significantly lower applied field than expected from previous scalings developed at lower β_N. However, if the effect of the plasma response in amplifying the error field calculated by IPEC is considered, a linear scaling of the threshold perturbation with density is restored, as shown in Fig. 1.

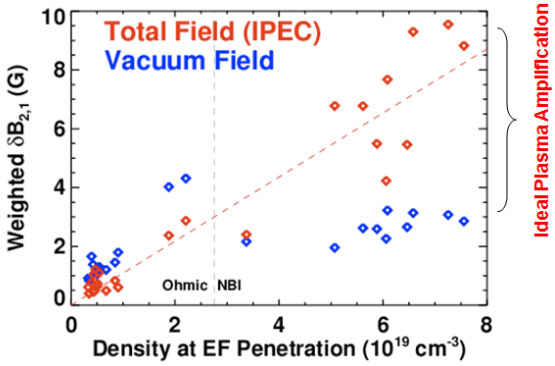

Fig.1: Scaling showing the density threshold for error field penetration for the vacuum error field case and the total error field that includes the plasma amplification of the error field.

2.4 Physics of Neoclassical Tearing Modes

The difference in aspect ratio between NSTX and DIII-D, has enabled the aspect-ratio scaling of the marginal island width for growth of the n=1 neoclassical tearing mode (NTM) to be determined. The destabilization of NTMs involves the physics of small island threshold effects and seeding of the initial perturbation. The physics of the small island stabilizing terms was investigated in NSTX by generating an NTM at high beta and reducing beta to the "marginal point" where the small-island effects just balance the sum of the classical stability, the curvature, and the helically perturbed bootstrap current. At beta below this balance, self-stabilization of the NTM occurs. Comparison of the "offset" conditions for the n=1 NTMs between DIII-D and NSTX shows that the marginal island width generally scales with the ion banana-orbit width (proportional to $3\cdot\varepsilon^{1/2}\cdot\rho_{\theta i}$, where $\rho_{\theta i}$ is the ion poloidal gyro-radius) at the resonant q = m/n surface.

NTMs are a particular concern for future low rotation devices, as the β limits for their destabilization are known to fall with decreasing rotation. This physics was explored by utilizing independent n = 1 and n = 3 field perturbations to brake the plasma by both resonant and non-resonant means, studying the effects on both rotating 2/1 NTM thresholds and on the ultimate locked mode threshold. Results showed that both n = 1 and n = 3 fields led to significant braking at similar magnitudes of applied perturbations, lowering bootstrap thresholds to rotating modes, and leading to locked modes if rotation braking was more than 50%. Results showed no correlation with rotation of the bootstrap drive for the mode at time of onset, but did show a significant trend with local rotation shear. This

suggests that plasma rotation acts on mode thresholds through changes to the intrinsic tearing stability (Δ'). This suggests that strategies to avoid or control the NTM should focus on manipulation of this quantity through, for example, modifications to the current or rotation profile.

2.5 ELM Pacing with Non-Axisymmetric Coils

In NSTX, ELM pacing with periodic pulses of non-axisymmetric (typically, n = 3) field perturbations using the RWM coils has been shown to be effective at preventing impurity accumulation while retaining high confinement. For a pacing frequency of 30 Hz the stored energy decrement from the triggered ELMs is small, 10 – 15%, while the radiated power at the end of the current flat-top is reduced by a factor of 3. By increasing the triggering frequency to 50 Hz, the ELM size, expressed as the fraction of plasma energy lost at each ELM, can is reduced to ~5% [12]. In addition to ELM pace-making with pulse Resonant Magnetic Perturbations (RMP), a scenario was developed with ELM pace-making via vertical jogs of the plasma [13]. ELM pacing at 30 Hz was observed with the ELMs synchronized to the plasma vertical motion. A reduction of the ELM size with increasing jog frequency was observed. Application of a steady state n = 3 field allowed ELMs to be triggered with smaller jogs.

3. Transport and Turbulence in Plasmas

3.1 L-H Threshold studies in support of ITER

In NSTX helium plasmas heated by deuterium NBI, it was found that P_{LH}/n_e was nearly identical to that in deuterium plasmas. Since results from other experiments have shown that hydrogen plasmas have threshold powers nearly twice that for deuterium, the NSTX results suggest that operation in helium may be a better approach to developing H-mode scenarios in the early non-nuclear phase of ITER operation.

Other experiments were performed to measure the dependence of the L→H transition on applied 3D non-axisymmetric field amplitude. It was found that P_{LH}/n_e is significantly, ~65%, higher with higher applied n = 3. However, the difference in the rotation does not appear to be the dominant factor, which is consistent with earlier comparisons of the threshold between plasmas heated by HHFW and NBI power. It was found that P_{LH}/n_e was almost a factor 2 higher for 1 MA plasma current than for 0.7 MA, indicating a strong dependence on plasma current. Lithium coating of the PFCs was found to reduce the power threshold in NBI-heated plasmas from 2.7 MW without lithium to 1.4 MW with lithium applied, corresponding to a reduction in P_{LH}/n_e by ~30% from 0.9 to 0.6 MW/10^{19}m^{-3}. In experiments with the toroidal magnetic field (TF) reversed so that the $B \times \nabla B$ particle drift for the ions changed from being towards the lower divertor to being towards the upper divertor; the plasma current direction was unchanged, it was found that the L-H threshold in the loss power ($P_{loss}= P_{OH} + P_{aux}$ - dW/dt) for upper single null discharges was lower by about 40% than for lower single null discharges. Furthermore, when lithium was used to coat the lower divertor, this reduction approximately doubled, confirming the large impact lithium has in reducing the threshold power. Motivated by recent calculations with the XGC code [19], an experiment to measure the L→H power threshold was conducted for two different triangularities (δ) at roughly constant X-point height. The power threshold was 20-30% lower at the lower δ, qualitatively consistent with the XGC-O calculations indicating a larger radial electric field and gradient at low δ.

3.2 Dependence of momentum pinch velocity on collisionality

Theory has recently suggested a relatively weak dependence of the momentum pinch on collisionality. It is critical to validate this, since a degradation of the pinch at low collisionality would be unfavorable for producing peaked rotation profiles in future burning plasma devices such as ITER, which will have small external momentum input. In NSTX, the braking torque from the application of non-resonant magnetic perturbations was used to modify the gradient in the toroidal velocity differently from the change in the velocity itself. The diffusive and pinch contributions to the transport were then determined by modeling the toroidal angular momentum flow through each radius inferred from the measured rotation data, and the momentum source from the NBI calculated by TRANSP. A non-linear least squares fit was used to determine an assumed time-independent momentum diffusivity χ_ϕ and a momentum pinch velocity V_{pinch} that best reproduced the time history

of the toroidal angular momentum profile. The collisionality was varied while maintaining other dimensionless quantities as close to constant as possible. In general, the inward pinch velocity is found to decrease as the collisionality is reduced. A similar trend has also been seen on DIII-D, with a clear reduction in the pinch velocity with collisionality. Hence, the data suggest that there is some commonality in the mechanisms responsible for the momentum pinch at both low and conventional aspect ratio [14]. In terms of peaking the rotation profile, the ratio of the pinch to the momentum diffusivity is more important than the absolute pinch velocity. This too shows a strong dependence on collisionality [14].

3.3 Electron thermal transport

Previous experiments in NSTX identified a correlation between fast particle modes identified as Global Alfvén Eigenmodes (GAEs) and increased electron thermal transport in the core of NSTX plasmas. In a recent study, a reference discharge was produced, and the neutral beam power varied to modify the character and amplitude of the GAE activity. A key addition to this experiment was the inclusion of inteferometric data from the high-k scattering diagnostic [15] which measured line integrated density fluctuations at a tangency radius of ~115 cm, near the predicted peak of the GAE mode structure, and at a tangency radius of ~120 cm, where the GAE mode amplitude is predicted to be lower by an order of magntitude. Results indicate increased electron transport with increased GAE activity. For r/a < 0.5, theoretical calculations of the predicted transport using the measured density fluctuations from line-integrated interferometric measurements have fallen short of the TRANSP inferred values of χ_e by factors of 4 to10. However, further analysis of the GAE measurements using high-frequency magnetic pickup coils has revealed a 'bursting' character of the modes, which indicates that the peak magnitude of the GAE density fluctuations may be far higher than the time-averaged values used in the transport calculations. Additionally, numerical calculations show that the GAE-induced χ_e can scale quite strongly with mode amplitude, $\chi_e \sim \alpha\text{^}3 - \alpha\text{^}6$, as the modes begin to overlap and cause stochastic transport.

The source of anomalous transport in fusion plasmas is thought to be microturbulence. In NSTX, electron gyro-scale density turbulence is studied by using a tangential 280 GHz microwave scattering system (high-k scattering system) [16]. The high-k scattering system has five channels capable of covering k_r from 5 cm^{-1} to 20 cm^{-1} with a resolution of 0.7 cm^{-1}, and thus a 1D k spectrum in the 2D $k_\perp$ space can be obtained, where $k_\perp$ denotes wavenumber perpendicular to the equilibrium magnetic field. A recent focus of the study of high-k turbulence has been the shape of the k spectrum. The k spectra in previous publications have monotonic power laws with no sign of saturation of spectral power at small wavenumbers [17 18]. Improvements to the high-k scattering system this year allowed simultaneously obtaining scattered light with all five channels in contrast to at most three channels in the past. In recent experiments, saturation of the spectral power at small wavenumbers has been observed for $k_\perp\rho_s < 6$ for L-mode plasmas and for H-mode plasmas $k_\perp\rho_s < 10$. The k spectrum of a L-mode plasma was compared with a H-mode plasma with identical I_p, B_T and neutral beam power, and it was found that although the spectra come close to each other at $k_\perp\rho_s > 10$, the spectral power of the H-mode plasma at $k_\perp\rho_s < 10$ can be smaller than that of the L-mode plasma by two orders of magnitude. The dramatic difference in spectral power at small wavenumber between L-mode and H-mode plasmas is consistent with long wavelength turbulence being more important in driving anomalous transport and indicates that electrostatic turbulence could be responsible for the observed anomalous transport [19].

3.4 Observation of improved performance regimes

A new high performance regime ("Enhanced Pedestal" or EP H-mode) has been observed in NSTX discharges, where the H-mode edge 'pedestal' temperature doubles and the energy confinement increases by 50%. The spontaneous transition is triggered by a large ELM, either natural or externally triggered by 3-D fields. The transport barrier grows inward from the edge, with a doubling of both the pedestal pressure width and the spatial extent of steep radial electric field shear. The resulting discharge has a 50% increase in energy confinement time up to 1.8*ITER98y2 H-mode scaling, a β_N up to 6.5 maintained for 3 energy confinement times [20].

4. Plasma Boundary Physics

4.1 Studies of Heat Fluxes in the Scrape-off Layer and to the Divertor Surface

The peak heat flux at PFCs is intimately tied to the downstream deposition footprint on both the scrape-off layer (SOL) and private-flux region sides, which in turn are related to cross-field transport and the upstream midplane profile widths. The dependence of the lower divertor heat flux profiles on P_{NBI}, I_p, B_T, and lithium conditioning in H-mode discharges was measured with IR thermography. Previously we reported that the SOL heat flux widths (λ_q^{mid}, i.e. divertor profile width magnetically mapped to the midplane) decreased with I_p, and were relatively independent of P_{NBI} at high P_{NBI} at low δ ~0.4. Experiments over the past two years were extended to higher δ ~0.7, showing that λ_q^{mid} scales as $I_p^{-1.6}$, and largely independent of P_{NBI} and B_T. [21]. In addition, when lithium coatings resulted in ELM-free discharges, there was a further contraction of λ_q^{mid} by about 50%. At constant δ, the λ_q^{mid} was relatively independent of the magnetic flux expansion in the range of 10 – 40, leading to a strong reduction of the peak heat flux with increasing flux expansion because the λ_q^{div} increased linearly with flux expansion. Numerical simulations [22] using a reduced turbulence model have shown that some of the observed scaling of λ_q^{mid} with P_{NBI} and I_p is due to intermittent separatrix-spanning convection.

Externally imposed non-axisymmetric magnetic perturbations are observed to alter divertor heat and particle flux profiles. The divertor profiles are found to have a modest level of multiple local peaks, characteristic of strike point splitting or the 'magnetic lobe' structure, even before the application of the 3D fields in some discharges, thought to be due to intrinsic error fields. The applied 3D fields substantially augmented the striations from the intrinsic strike point splitting, amplifying the local peaks and valleys. The measured heat flux profile shows that the radial location and spacing of the striations are qualitatively consistent with a vacuum field tracing calculation [23].

4.2 "Snowflake" divertor configuration development

The compact geometry of the ST divertor and the requirement of low density (n_e/n_G ~ 0.5 – 0.7, where n_G is the Greenwald density limit) operation for high neutral beam current drive efficiency define a unique edge plasma regime which will place greater demands for handling the divertor and first-wall particle and heat fluxes. In support of this need, a novel divertor configuration, called the "snowflake" divertor (SFD), has been tested on NSTX. The SFD uses a second-order X-point created by merging, or bringing close to each other, two neighboring first-order X-points. Experiments conducted on NSTX obtained a SFD plasma configuration with a minimal set of two divertor coils (Fig. 2) for periods of hundreds of milliseconds and confirmed many of the predicted SFD benefits [24]. When compared to a similar medium triangularity (δ = 0.5 - 0.65) standard divertor discharge in NSTX, the SFD maintained H-mode properties without any degradation of stored energy and confinement. Divertor heat flux profiles showed a large reduction in peak heat flux during the SFD periods. Divertor radiation due to carbon impurity was significantly increased in the SFD. A large volume recombination region with T_e ~ 1.5 eV, $n_e > 3 \times 10^{20}$ m^{-3} developed, while ion flux to the divertor plate was reduced, suggesting an extended region of detachment in the divertor. As in previous divertor detachment experiments in NSTX [25], the core carbon density was reduced by up to 50%.

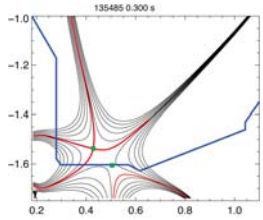

Fig. 2 – The snowflake divertor configuration in NSTX.

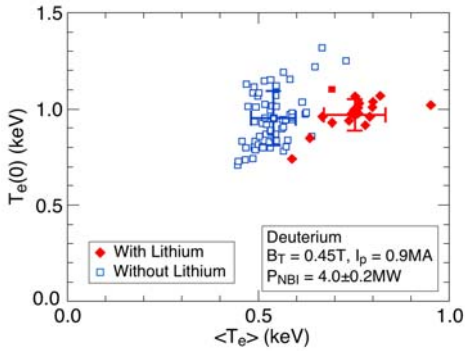

Fig.3. Central Te vs. volume averaged Te for plasmas with and without lithium evaporated on the graphite PFCs under otherwise similar conditions.

4.3 Lithium Research

Evaporative Li coatings: Research into the effects of lithium–coated PFC has been continued in NSTX using the two lithium evaporators (LITERs) [26,24].

In one dedicated experiment, lithium was evaporated onto the lower divertor, in increasing amounts at evaporation rates from 16 to 50 mg/minute, applied for 10 or 8 minutes, before each high-elongation, high-triangularity, I_p = 1 MA discharges with 5 MW NBI heating. At the same time, the pre-deposition period of helium glow-discharge cleaning (HeGDC) was gradually decreased from 10 to 4 minutes and finally eliminated altogether. Even relatively thin lithium coatings (e.g. 200-300 mg lithium deposited over roughly 2 m^2) significantly reduced the density in the early part of discharges, produced earlier H-mode transitions, and increased the electron temperature, electron stored energy and confinement time. As the lithium deposition increased, the discharges became increasingly ELM-free, and finally, fully ELM-free. The discharge pulse length increased to about 1.2 s with lithium and with n = 3 error-field correction and n = 1 RWM feedback applied. Emission from OV and the ratio of OV to CIII line emission decreased. An H-mode discharge was obtained with only 1 MW NBI (1.8 MW total power). As a result of increasing lithium wall coatings, recycling and edge fueling were reduced, which relaxed the edge density profile gradients. In contrast, the edge T_e profile was unaffected in the H-mode pedestal steep gradient region at constant plasma stored energy; however, the region of steep T_e gradients extended radially inward by several cm following lithium coatings. Consequently, the pressure profile width and pedestal height increased substantially [27].

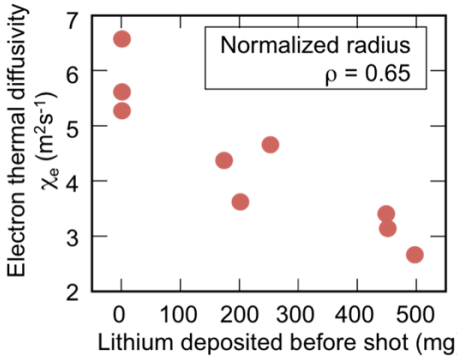

Fig.4. TRANSP results for the electron thermal diffusivity as lithium deposition was increased with other conditions held

The improvement in electron stored energy occurred as a result of a broadening of the electron temperature profile, as shown in Fig.3. The transport analysis code TRANSP [28] shows that the electron thermal transport in the outer region of the plasma is progressively reduced (Fig.4) as lithium deposition increases [26]. The thermal ion confinement remains close to the neoclassical level both with and without lithium, although the fast-ion contribution to total energy increases as a result of the higher average electron temperature. With improvements in confinement and suppression of ELMs, there was a significant secular increase in the effective ion charge Z_{eff} and the radiated power in H-mode plasmas as a result of increases in the carbon and medium-Z metallic impurities. Lithium itself remained at a very low level in the plasma core, <0.1%.

Liquid Lithium divertor (LLD): A LLD assembly was installed recently on the outer part of the lower divertor of NSTX [26]. The LLD consists of four plates, each 20 cm wide and spanning 80° toroidally mounted flush with the surrounding graphite tiles of the outer divertor plates and centered at a major radius of 0.75 m. The plasma-facing surface of the plates is coated with a 165 μm thick layer of molybdenum with 45% porosity, plasma sprayed on a protective barrier of 0.25 mm stainless steel, that is bonded to a 2.2 cm thick copper substrate. The plates can be heated by embedded electric heaters and cooled by passing compressed air through an embedded gas line. Lithium was applied to the LLD, and simultaneously to the surrounding graphite PFCs also, using the LITER system. With the LLD at initial temperatures in the range from 50 to 300°C, the amount of gas fueling required to prevent locked-modes during plasma startup and to maintain reproducible discharges, both indicators of the overall PFC-pumping ability, was similar to that for solid lithium coatings on graphite. The duration of lithium pumping (as indicated by maintaining ELM-free H-modes with lower edge density and higher edge temperature) for a fresh thin lithium coating (500–1000 nm) for the outer strike point on either the graphite inner divertor or the LLD was 2-3 discharges. However, the duration of lithium pumping was ~100 discharges after more than 260 g of lithium had been evaporated onto the lower PFCs, filling the porous molybdenum surface of the LLD to ~35% of its nominal capacity.

Diffusive Li deposition: In order to extend lithium coverage to a larger fraction of the NSTX PFCs, a new method was tested in which LITER was used to evaporate lithium into low pressure helium gas. The mean free path of Li atoms in He was varied by changing the helium pressure to produce a diffusive coating of the upper vessel, midplane and regions not in line-of-sight to one of the LITERs.

Monte-Carlo modeling was used to derive a sequence of helium pressures to vary the lithium mean free path for optimal uniformity of lithium coverage of the PFCs. The increased lithium coverage of the vessel, which was evident in 2D camera images of LiII 5485 Å line emission from the plasma chamber, resulted in strong wall pumping and necessitated the increase of deuterium fueling to very high levels [26].

Deuterium retention during and after plasma discharges: The processes governing deuterium retention by graphite and lithium-coated graphite PFCs were investigated in dedicated experiments involving measurements of the dynamic gas balance and analysis of the surface composition. In plasmas heated by NBI, the deuterium retention by the lithium-coated graphite was ~93%, but the uncoated graphite retained somewhat less, ~87%. Both with and without lithium, the retained deuterium was released as gas on timescales ranging from seconds to weeks or longer.

5. Wave-Particle Interactions in Plasmas

Improved high harmonic fast-wave heating performance and understanding: The NSTX High-Harmonic Fast-Wave (HHFW) system is aimed to heat electrons and ramp-up and sustain plasma current non-inductively. The system consists of a twelve-element antenna fed by six power amplifiers operating at 30 MHz with total available power P_{RF}=6 MW [29]. The phasing of RF waves between adjacent straps controls the wavenumber parallel to the magnetic field of the waves coupled to the plasma. Recent modifications of the antenna to increase the maximum arc-free power coupled to the plasma led to exceeding previous performances. A record T_e=6.2 keV was achieved in helium L-mode plasmas with P_{RF}=2.7 MW, representing a 30% increase in heating efficiency ($dT_e(0)/dP_{RF}$) compared to previous results. Moreover, a central T_e>3.5 keV was sustained with P_{RF}=2.7 MW for 0.3 s, much longer than previously achieved. Progress was made in understanding the interaction of RF with the fast-ions from NB injection. The Fast-ion D-alpha (FIDA) diagnostic [30] measured changes in the fast-ion density during HHFW heating [31]. An increase by a factor ≥2 was measured near the magnetic axis (7^{th} and 8^{th} deuterium cyclotron harmonics), gradually decreasing near the plasma edge (11^{th} harmonic). Significant differences are observed between the measured fast-ion profiles and calculations from the CQL3D code. The peak in the predicted fast-ion density is 3 times higher and much more localized than the measured value. The cause of this discrepancy is likely to be the zero ion-banana-width approximation used in CQL3D [32], whereas this parameter is large on NSTX, in the range 10 – 15 cm. Finite banana-width effects are being incorporated into CQL3D and the complementary AORSA RF-absorption code to improve their predictive capability for fast-ion interactions with the HHFW in NSTX.

Study of Alfvénic instabilities and associated fast-ion transport: Alfvénic instabilities (AEs) routinely observed during NBI on NSTX have frequencies from 10-200 kHz for toroidal Alfvén eigenmodes (TAEs) and energetic-particle modes (EPMs) up to ~2 MHz for GAEs/CAEs. Recent experiments have mainly focused on the interaction between TAEs/EPMs and fast ions, which is thought to be the main fast ion loss mechanism in future devices such as ITER [33]. Fast ion losses induced by bursting TAE *avalanches* [34] have been extensively documented in L-mode plasmas [35]. It is found that TAEs can efficiently deplete up to ~30% of the fast ion population over a significant portion of the minor radius. The losses increase with the modes' amplitude [34]. In contrast, no clear evidence of losses associated with higher frequency AEs has been found. However, a correlation between GAE bursts and TAE avalanches is observed, suggesting that GAEs may cause a redistribution of fast ions that, in turn, can trigger the avalanches [36]. The fast ion losses caused by TAE avalanches have been successfully modeled [34,36] through the ORBIT code [37], using the mode structures calculated by the NOVA code [38]. The mode structures are selected and re-scaled to match the mode structure measured by reflectometers. New experiments will extend TAE studies to H-mode scenarios. In parallel, validation of self-consistent, non-linear codes (e.g. M3D-K, [39]) is being pursued to improve the predictive capability of AE's dynamics, including associated fast ion transport and non-linear phenomena, toward next generation devices and ITER.

6. Plasma Startup without Reliance on a Central Solenoid

In the ST configuration there is little room for a central solenoid to initiate and sustain the plasma by induction, as is usually done in a conventional tokamak with higher aspect ratio. Although NSTX is

equipped with a central solenoid, it is also exploring several approaches to starting and sustaining plasmas in the ST without relying solely on it. The primary non-inductive startup technique in NSTX is Coaxial Helicity Injection (CHI) which involves using a power supply to create a discharge carrying poloidal current between the inner and outer divertor annuli of NSTX which are insulated from each other [40]. In the presence of a toroidal field, the current carried by the plasma, which flows along magnetic field lines, develops a strong toroidal component. Through the process of magnetic reconnection, that toroidal current can be transferred from the open magnetic field lines connecting the divertor electrodes to the closed, nested flux surfaces of a standard tokamak equilibrium.

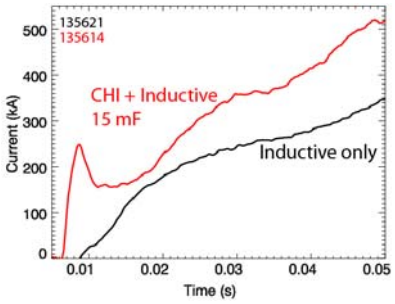

Fig. 5. Plasma current traces from a discharge started with and without CHI. Both use the same pre-programmed inductive flux.

Previously, up to 50 kA of toroidal plasma current produced by CHI was successfully coupled to inductive ramp-up in NSTX. These discharges when heated with NBI achieved plasma temperatures over 0.8 keV and transitioned to the H-mode, demonstrating the compatibility of CHI start-up with standard plasma operation. However, in these experiments, the CHI current that could be successfully coupled was limited by impurity production from the CHI electrodes and the occurrence of absorber arcs (*i.e.* parasitic discharges across the insulating gap in the upper divertor). Extensive conditioning of the divertor plates that serve as the electrodes for the CHI discharge greatly reduced impurity production during CHI [41]. Further, by energizing, for the first time, the axisymmetric absorber field-nulling coils located near the upper divertor in NSTX, the absorber arcs could be delayed or suppressed. These improvements increased the current at the hand-off from CHI to induction to nearly 200 kA. Later in the inductive ramp-up, the discharges with CHI applied reached significantly higher plasma current than discharges with only the inductive loop voltage applied. For example, in discharges with identical programming of the central solenoid current, the plasma current at t = 50 ms (the CHI is applied only to t ≈ 15 ms) increased from 340 kA with induction only to 520 kA with CHI (Fig. 5). This represents a poloidal flux saving equivalent to 180 kA of plasma current which is ~25% of the flat-top current of 700 kA typical of long-pulse scenarios on NSTX. The most recent experiments [40] in which CHI initiation was followed by inductive ramp-up produced produced final currents exceeding 1 MA using only 0.28 Wb of the 0.33 Wb of the inductive flux available from a uni-directional swing of the central solenoid. This is the highest current produced in NSTX using this amount of central solenoid flux, and is a significant improvement over the 800 kA achieved using all of the flux from a single swing of the central solenoid in 2009 and described in [41]. These plasmas have both a very high elongation of $\kappa \approx 2.6$ and, as a result of the hollow electron temperature profile and rapid inductive ramp, very low internal inductance $l_i \approx 0.3$ from the start of the discharge. Finally, these plasmas are relatively free of MHD activity despite having low density, which has previously been associated with increased instability during normal inductive startup. TSC simulations indicate that these targets should be capable of reaching a high fraction of neutral beam driven current. Thus, the 2010 campaign has not only significantly improved CHI startup capability, but also produced the type of plasmas that are needed to meet the objectives of the non-inductive start-up and ramp-up program of NSTX.

7. The Development of Integrated High-Performance Scenarios

A major goal for NSTX research is the achievement of high-β discharges which can be maintained non-inductively for long pulses, eventually extending to several relaxation times of the current profile. To achieve this, it will be necessary to maximize the bootstrap current, and the current driven by the NB injection. Significant progress has now been made in increasing the bootstrap current and the pulse length in NBI-heated H-mode plasmas by a combination of techniques [42]. The first of these has been to raise the plasma elongation, κ, which increases the poloidal-beta β_P at fixed β_N.

Highly reliable scenarios with high-κ, and high-β_N that have 60 – 65% non-inductive current drive fraction have now been produced as shown in the black trace in Fig. 6. This B_T=0.48 T discharge achieved a maximum $\beta_P \approx 1.8$ and $\beta_P > 1.6$ for 0.5 s, with ~50% of the toroidal current driven by the plasma pressure, and ~20% by the neutral beams. It was limited in duration by the heating of the TF coil. By decreasing the toroidal field to B_T=0.38, the TF pulse was extended (blue trace) although the coil heating still limited the discharge length. Confinement in these discharges was increased by using lithium wall coating, and routinely achieved a global energy confinement time enhancement H_{98}=1 relative to the ITER-98 H-mode scaling expression. Both n=3 error field correction and n=1 feedback were used to maintain high plasma rotation and stabilize potential RWMs. These discharges were then extended to higher normalized current by further reducing the toroidal field and increasing the plasma current, as shown in the red trace in Fig. 6. This allowed sustained values of toroidal beta, β_T, approaching 25%. These higher β_T cases had non-inductive current fractions of almost 50%. Also noteworthy are the very high values of the parameter $\beta_N/l_i \approx 13$ (%.m.T/MA) achieved, compared to ~4 in conventional tokamaks. These discharges provide a test of MHD control techniques at parameters relevant to a future ST-based component test facility for fusion power development. The reliability of these high β_N/l_i scenarios has been shown to improve when the feedback control with n=1 mode detection using both B_P and B_R sensors near the outboard midplane of the plasma was utilized for the RWM control [1].

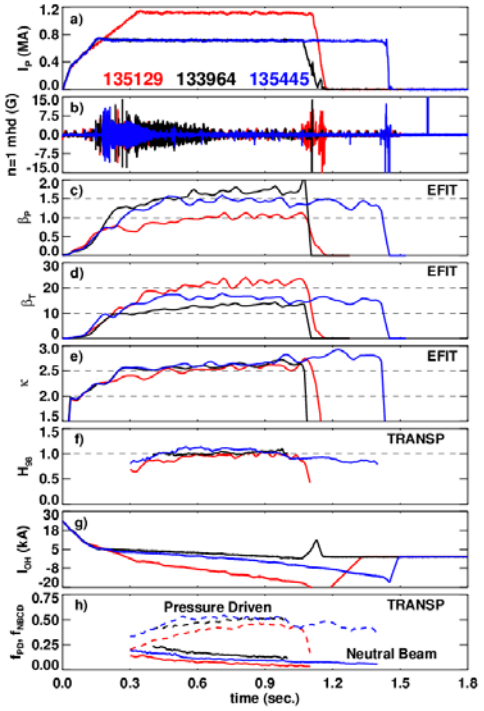

Fig. 6. High-k discharges designed to maximize the non-inductive fraction (black), the pulse length (blue), and β_T (red).

As shown in Fig. 7, discharges with loop voltages of only about 130 mV have been sustained for 0.9 s. These discharges had the lowest pulse-averaged flux consumption of any NSTX H-mode plasma to date: at the end of the toroidal field pulse, again imposed by the coil heating, most of these discharges had used only half of the available transformer flux of 0.7 Wb. These high-κ, high-β scenarios, which are the culmination of a continuing effort to achieve sustained high-elongation operation, represents a substantial extension of the operational space available in NSTX and will serve as the basis for the NSTX upgrade and also for future ST devices.

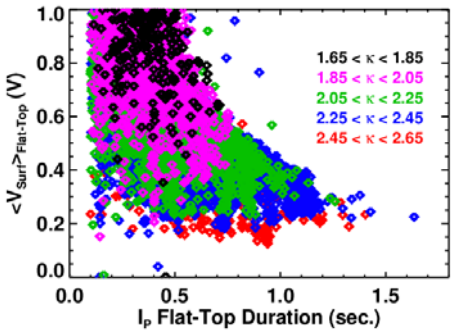

Fig. 7: Pulse averaged surface voltage versus the current flattop duration, sorted by the plasma boundary elongation. Increases in the achievable elongation have led to a factor of ~2 reduction in the surface voltage.

NSTX has also benefited from substantial improvements in plasma shape control in the past two years [43]. Controllers have been developed to regulate both the radius of the outer strikepoint (on the lower horizontal divertor target) and the height of the inner strikepoint (on the lower vertical target). These controllers were used to provide the basic configuration for LLD studies and to create snowflake divertors. A controller was also developed to regulate the outer strikepoint radius and X-point height, and the

relative merits of these two approaches remain under study. Finally, initial studies of the effect of the plasma squareness on transport and global stability have begun.

[1] S.A. Sabbagh, et al., EXS/5-5, this conference paper
[2] S.A. Sabbagh, et al., Nucl. Fusion **50** (2010) 025020.
[3] J.E. Menard, et al., Nucl. Fusion **47** (2007) S645
[4] S.P. Gerhardt, et al.,Plasma Phys. Control. Fusion **52**, 104003 (2010)
[5] O.N. Katsuro-Hopkins, S.A. Sabbagh, J.M. Bialek, Proc. 48th IEEE Conf. on Decision and Control. Shanghai, China, (2009) p 309.
[6] J.W. Berkery, et al., Phys. Rev. Lett. **104**, 035003 (2010).
[7] A.M. Garofalo, et al., Nucl. Fusion **47** (2007) 1121.
[8] J.W. Berkery, et al. Phys. Plasmas **17** (2010) 082504.
[9] B. Hu, R. Betti, J. Manickam, Phys. Plasmas **12** (2005) 057301.
[10] H. Reimerdes, et al., Phys. Rev. Lett. **93**, 135002 (2004)
[11] J-K Park, et al., Phys. Plasmas **16**, 056115 (2009)
[12] J.M. Canik, et al., Phys. Rev. Lett. **104** (2010) 045001, J.M. Canik, EXC/8-1, this conference paper
[13] S.P Gerhardt, et al., Nucl. Fusion **50**, 064015 (2010)
[14] W.M. Solomon, et al., Phys. Plasmas **17**, 056108 (2010)
[15] E. Mazzucato, Plasma Phys. Control. Fusion **48**, 1749 (2006).
[16] D.R. Smith, et al., Rev. Sci. Instrum. **79** (2008) 123501
[17] E. Mazzucato, et al., Phys. Rev. Lett., **101** (2008) 075001
[18] D.R. Smith, et al., Phys. Plasmas **16** (2009) 112507
[19] S.M. Kaye, EXC/2-3Rb and W. Weixing, THC/P4-30, this conference paper and C.S. Chang, et al., Phys. Plasmas **11** (2004) 2649
[20] R. Maingi, et al, Phys. Rev. Lett. **105** (2010) 135004
[21] T.K. Gray, et al., EXD/P3-13, this conference paper
[22] J.R. Myra, et al., to be publ. in J. Nucl. Mater. [lodestar.com/LRCreports/Myra_PSI2010_SOL_width.pdf]
[23] J-W. Ahn, et al., Nucl. Fusion **50** (2010) 045010; J-W. Ahn et. al., EXD/P3-01, this conference paper
[24] V. Soukhanovskii, et al., EXD/P3-32, this conference paper
[25] V.A. Soukhanovskii, et al., Phys. Plasmas **16** (2009) 022501.
[26] H.W. Kugel, FTP/3-6Ra, this conference paper and C.H. Skinner, et al., J. Nucl. Mater. (2010) in press
[27] R. Maingi, et. al., Phys. Rev. Lett. **103** (2009) 075001, R. Maingi, et al., EXD/2-2, this conference paper
[28] R. J. Hawryluk, et al., "An Empirical Approach to Tokamak Transport", in Physics of Plasmas Close to Thermonuclear Conditions, ed. by B. Coppi, et al., (CEC, Brussels, 1980), Vol. 1, pp. 19-46.
[29] G. Taylor, et al., Phys. Plasmas **17**, 056114 (2010)
[30] M. Podesta, et al., Rev. Sci. Instrum. **79**, 023502 (2008)
[31] D. Liu, et al., Plasma Phys. Control. Fusion **52**, 025006 (2010)
[32] M. Choi, et al., Phys. Plasmas **17**, 056102 (2010)
[33] A. Fasoli, et al., Nucl. Fusion **47**, S264 (2007)
[34] E. Fredrickson, et al., Phys. Plasmas **16**, 122505 (2009)
[35] M. Podesta, et al., Phys. Plasmas **16**, 056104 (2009)
[36] E. Fredrickson, et al., EXW/P7-06 and M. Podesta, et al., EXW/P7-23, this conference paper
[37] R. White, et al., Phys. Fluids **27**, 2455 (1984)
[38] C. Cheng, Phys. Rep. **211**, 1 (1992)
[39] J. Lang et al., Phys. Plasmas **16**, 102101 (2009)
[40] B.A. Nelson, et al., EXW/P2-08, this conference paper
[41] R. Raman, et al., Phys. Rev. Lett. **104** (2010) 095003
[42] S.P. Gerhardt, et al., EXS/P2-08, this conference paper
[43] E. Kolemen, et al., EXD/P3-18, this conference paper and E. Kolemen, et al., Nucl. Fus. **50**, 105010 (2010)

This work performed under the auspices of the U.S. Department of Energy by Lawrence Livermore National Laboratory under Contract DE-AC52-07NA27344.